

THE PRESENT WORK WAS SUBMITTED TO THE DEPARTMENT OF CONTINUUM
MECHANICS

RHEINISCH-WESTFÄLISCHE TECHNISCHE HOCHSCHULE AACHEN
FACULTY OF MECHANICAL ENGINEERING

MASTER THESIS

NONLINEAR MATERIAL PARAMETER IDENTIFICATION OF SOFT MATERIALS BASED ON AN INVERSE FINITE ELEMENT METHOD APPROACH

Presented by:	Nadia Pinedo Oruna, B.Sc.
Study programme:	General Mechanical Engineering M.Sc.
Matriculation number:	397 011
Reviewer:	Univ.-Prof. Dr.-Ing. Mikhail Itskov
Supervisor:	Rasul Abdulsalamov, M.Sc.
External supervisor:	Prof. Kazumi Matsui

Declaration of Authorship

I declare that this work has been composed by myself, and describes my own work, unless otherwise acknowledged in the text.

All sentences or passages quoted in this paper from other people's work have been specifically acknowledged by clear cross-referencing to author, work and page(s). Any photos and illustrations which are not the work of the author have been used with the explicit permission of the originator and are specifically acknowledged.

This work has not been and will not be submitted for any other degree or the obtaining of ECTS points at the RWTH Aachen University or any other institution of higher education.

Aachen, 25th of May 2023

Nadia Pinedo Oruna, B.Sc.

Contents

1	Introduction	1
1.1	Background and Problem Statement	1
1.2	Objective and Scope of the Study	1
1.3	State of the Art	2
1.3.1	Experimental Characterization for Soft Materials	2
1.3.2	Material Modeling of Soft Materials	9
1.3.3	Inverse Finite Element Method for Parameter Identification	15
1.4	Overview	17
2	Experimental Model	19
2.1	Experimental Model I	20
2.2	Experimental Model II	22
2.3	Experimental Tests Description	24
2.4	Analysis and Overview of the Data and Results	26
2.4.1	Middle Point	27
2.4.2	Load-Unloading	28
2.4.3	Nearby Point	29
2.5	Main Assumptions for Material Modeling	32
2.5.1	Level 1: Linear elasticity	33
2.5.2	Level 2: Hyperelasticity	33
3	Computational model	35
3.1	Middle point	35
3.1.1	Description	35
3.1.2	Analysis and Complications	35
3.1.3	Verification of the Simulation Model	35
3.2	Nearby point	35
4	Inverse Finite Element Method for Material Parameter Identification	37
4.1	Procedure of IFEM	37
4.2	Material Modeling	37
4.2.1	Response Surface Optimization	37
4.2.2	Objective Function Optimization	37
4.2.3	Analysis and Comparison of Each Approach	37
5	Results	39
5.1	Overview and Analysis	39
5.2	Framework proposal	39
5.3	Verification and Validation	39
5.3.1	Deeper indentation	39
5.3.2	Deformation profile analysis	39
5.4	Limitations and implications of the results	39
5.4.1	First Experimental model	39

5.4.2	Second Experimental model	40
5.5	Material model framework assumptions	40
5.5.1	First Material model	41
Linear elasticity	41	
Hyperelasticity	41	
5.6	Computational model	41
5.7	Material model	41
6	Conclusion and Outlook	43
6.1	Summary and Contributions	43
6.2	Recommendations for Future Research	43
6.3	Conclusions and Final Remarks	43
A	Frequently Asked Questions	45
A.1	How do I change the colors of links?	45
	Bibliography	47

List of Figures

1.1	Uniaxial tensile testing of ether-based polyurethane, Kanyanta and Ivankovic [16]	3
1.2	Uniaxial compression testing setup based on the book by Bergström [3]	5
1.3	Uniaxial compression testing methodologies showed by Griffin et al. [12]	6
1.4	Nanoindentation	7
1.5	Indentation testing: Diagram of static and mobile indentation tests, indenters were attached to a load cell, which was connected to a displacement transducer. Diagrams are based on the study made by Carter (2001) [4].	8
1.6	aspiration	9
2.1	First experimental model: Tensile and compression machine with an indenter with a rounded head. Test Specimen made from ultra-soft polyurethane resin positioned on a fixed platform with a similar shape for constraint.	20
2.2	First experimental model: Specimen dimensions made from ultra-soft polyurethane resin for indentation test.	21
2.3	YNU experimental model: 6-axis sensor Test Specimen made from ultra-soft polyurethane resin positioned on a fixed platform with a similar shape for constraint.	23
2.4	YNU experimental model: Loading diagram showing initial position of the indenter in normal position [20].	23
2.5	Middle test point: Loading point (Red point) on the top surface of the specimen.	24
2.6	Load-Unload Case: Experimental model I with modified configuration setup, on top of the movable crosshead a displacement transducer was equipped to capture unloading data.	25
2.7	Nearby test point: Loading points for each experimental model to analyze shear stresses and to validate the computation models.	26
2.8	Load-displacement curve experimental data for Middle Point use case for both experimental models.	27
2.9	Total Force Reaction-Displacement curve: Comparison between experimental data for Middle Point use case from both models.	28
2.10	Load-displacement curve experimental data for Load-Unload use case for both experimental models.	29
2.11	Load-Unload Use Case: Analysis of Viscoelastic material properties by using six different indentation speeds. Load-Displacement curves were obtained from the first experimental test configuration.	30

2.12 Total Force Reaction-Displacement curve: Comparison between experimental data for Middle Point and Nearby Point. This point was located 5 mm right from the midpoint, following the minor axis of the ellipsoid.	31
2.13 Nearby Point Use Case: Analysis of shear stresses by observing three different nearby points on the specimens surface. Load-Displacement curves were gathered from Experimental Model II showing each force component.	32
5.1 Expdata	40

List of Tables

List of Abbreviations

FEA	Finite Element Analysis
FEM	Finite Element Method
iFEM	inverse Finite Element Method
ASME	(The) American Society (of) Mechanical Engineering
TSSA	Transparent Structural Silicone Adhesive
PDMS	PolyDiMethylSiloxane
MAS	Minimal Access Surgery
FE	Finite Element
NH	Neo-Hookean
MR	Mooney-Rivlin
YM	Yeoh Model
OM	Ogden Model
RMSE	Root Mean Square Error
EPI	Experimental Model I
EPII	Experimental Model II
MP	Middle Point
LU	Load Unloading (Case)
NBP	Nearby Point

List of Symbols

A_b	cross-sectional area of the bar	m
A_s	cross-sectional area of the specimen	m
l_s	specimen gauge length	m
C_b	wave speed through the bar	m s^{-1}
v_{UC}	testing speed for compression test	m s^{-1}
E	Young's Modulus	MPa
S_{ijkl}	compliance tensor	
C_{ijkl}	stiffness tensor	
I_1^*	distortional first invariant	
I_2^*	distortional second invariant	
J	Jacobian of the deformation gradient	
b^*	left Cauchy-Green strain tensor	
I	identity matrix	
C_{10}, C_{01}	Mooney-Rivlin material parameter constants	
C_{10}, C_{20}, C_{30}	Yeoh model material parameter constants	
D_k	volumetric D-parameter	
F_s	simulated force	
F_e	experimental force	
n	number of data points	
r_{i1}	indenter head radius of experimental model I	
l_{i1}	indenter length of EPI	
r_1	specimen minor radius	
r_2	specimen major radius	
r_{t1}	specimen tumor minor radius	
r_{t2}	specimen tumor major radius	
r_{i2}	indenter head radius of experimental model II	
E_{i2}	Young's Modulus of indenter of EPII	
F_x	force reaction in X-direction of EPII	
F_y	force reaction in Y-direction of EPII	
F_z	force reaction in Z-direction of EPII	
h_I	indentation depth of EPI	
h_{II}	indentation depth of EPII	
p_{I1}	nearby point of EPI	
p_{II1}	first nearby point of EPII	
p_{II2}	second nearby point of EPII	
p_{II3}	third nearby point of EPII	
$u_{I_{MP}}$	maximum displacement of the middle point of EPI	
$F_{I_{MP}}$	maximum force of the middle point of EPI	
$u_{II_{MP}}$	maximum displacement of the middle point of EPII	
$F_{Z_{II,MP}}$	maximum force component in X-direction	
$F_{Y_{II,MP}}$	maximum force component in Y-direction	
$F_{X_{II,MP}}$	maximum force component in Z-direction	

$F_{I_{LU}}$	force of the loading-unloading case of EPI	
$F_{II_{LU}}$	force of the loading-unloading case of EPII	
$F_{I_{NBP}}$	maximum force component of nearby point of EPI	
$F_{II_{NB}}$	force component of nearby point of EPII	
A	contact area between specimen and indenter	
r_i	radius of the indenter	
F	applied indented force	
h	indentation depth	
C_1	material constant of hyperelastic model	
D_1	material incompressibility parameter	
J	determinant of the elastic deformation gradient	
I_1	first invariant of the right Cauchy-Green deformation tensor	
W	elastic strain energy potential function for the NH material	
K	initial bulk modulus	
$\sigma(t)$	stress	MPa (N mm ⁻²)
$\epsilon(t)$	strain	
ϵ_t	transmitted strain signal	
ϵ_r	reflected strain signal	
ϵ_{ij}	strain tensor	
σ_{ij}	stress tensor	
ν	Poisson's ratio	
δ_{ij}	Kronecker delta function	
μ	shear modulus	MPa (N mm ⁻²)
λ	Lame's constant	
κ	bulk modulus	MPa (N mm ⁻²)
ψ	Helmholtz free energy per unit reference volume	
σ	Cauchy stress	
λ_i	stretches of the deformation	
α_k	alpha-parameters	
ν_{i2}	Poisson's ratio of indenter of experimental model II	
σ	stress of linear elastic model	
ϵ	strain of linear elastic model	
λ	principal stretches	
μ	shear modulus or the second Lamé parameter	

1 Introduction

1.1 Background and Problem Statement

The biomechanical characterization of soft tissues has gained attention in medical research [7], in areas such as medical image analysis and visualization. For many years, the obtained medical diagnoses were often based on the assumptions of experts or their accumulated experience. While this information have proven to be useful in general, these methods have limitations in cases where quantifiable data is necessary, specifically for computer-assisted systems, e.g., medical diagnosis, therapy, and training [17]. To gather the material data, e.g., elasticity, stiffness, response under deformation and temperature, it is required to gain access to the soft tissues and perform *in vivo* testing experiments. However, obtaining accurate biomechanical data can be challenging due to the invasive nature of the procedures and the difficulty in maintaining constant and reproducible internal or external factors in experimental configurations [4].

Especially, when it comes to internal organs, obtaining reliable data for examination after their extraction is difficult because the material properties can vary between samples or testing locations on the same organ [5]. This is due to the influence of various factors such as changes in blood pressure, changes in material properties over time, symptoms of disease, and more. In addition, another problem is the lack of replication, due to the use of different individuals' organs, which introduces more external factors into the equation. Moreover, given a tissue sample, it is difficult to properly characterize the material due to its anisotropic property, which can lead potentially to inaccuracies in the result [7].

In the situation where the material data can be collected in a constant, fast and reliable process, a material model can be established and the computer-aided systems can predict the mechanical behavior of soft tissues, providing preoperative calculations. This demonstrates the importance of material data collection and material model development, especially in the context of computational models such as engineering simulation models created finite element analysis (FEA) software and their medical applications in medical devices, surgical procedures, and training softwares [4]. By using accurate material models, the accuracy of the simulation can be improved, aiding in a better understanding and predicting a soft tissue response to external stimuli [30], making them more useful in medical research and other related applications.

1.2 Objective and Scope of the Study

Soft materials, characterized by low elastic moduli and high sensitivity to external stimuli, frequently experience large deformation and display nonlinear responses [30], making the finite element method (FEM) a common approach for analyzing

these materials and solving continuum mechanical problems. Although FEM facilitates the analysis of complex structures with complex material behavior, simulating such materials requires high computational costs.

The main objective of this study is to identify the key parameters of soft materials and their influence on the development of a material model based on inverse finite element method (iFEM) approach. By identifying these key parameters, an attempt is made to approximate the behavior of complex materials through a simplified material model and assess its potential future applications in medical research and its use with organs.

To achieve this goal, an experimental configuration will be selected, and a computational model will be developed to use an iFEM approach to identify the key material parameters of the given soft material. With this method, it was possible to match the results of the computational model to the experimental data, and validate the model with additional data points.

The objective of this study is to develop a framework that identifies the essential material parameters of soft materials and evaluates their limitations and impact on a validated model, which can describe nonlinear material behavior. By contributing to this framework, the study aims to accelerate the development of material models for practical applications in medical research and development.

1.3 State of the Art

This section reviews the state of the art relevant to this study. First, the experimental characterization techniques are reviewed, including methods for obtaining mechanical and viscoelastic properties. This is followed by the description of different approaches to describe the material model for different soft materials. Then, the iFEM, which is one method to identify material parameters from experimental data, will be explained. Finally, the standard verification and validation process used in computational solid mechanics for medical devices based on the American Society of Mechanical Engineering (ASME) guidelines will be discussed. The goal of this chapter is to provide a comprehensive overview of the current methods use in the field and the identification of limitations and gaps in the current state of knowledge.

1.3.1 Experimental Characterization for Soft Materials

Experimental testing is a key approach to obtaining information about the mechanical behavior of soft materials. In order to characterize the mechanical behavior of a test specimen, the most common method method is to mechanically load the specimen and measure the response of the force against the displacement [3]. Soft materials are commonly applied for tissue engineering applications, however, some challenges arise for the design of experimental design due to their elastic modulus range (kPa) and complex mechanical properties [19].

Uniaxial Tension Testing

Uniaxial tension testing are widely employed to determine an stress-strain relationship. For uniaxial tension cases, a specimen is typically loaded by gripping the ends while applying tension, and the deformation is usually measured with a strain gauge



FIGURE 1.1: Uniaxial tensile testing: Diagram of three tensile testing of an ether-based polyurethane elastomer specimen done with three different experiment configurations for different strain rate analysis. Diagrams are based on the experiments made by Kanyanta and Ivankovic [16].

[3]. This kind of testing focuses on the central region of the specimen to evade complication arising from "edge effects". An homogeneous deformation in the central region is usually expected for this kind of testing, which simplifies the boundary problem and ensures that the measurements represents valid stress-strain values. However, there are two key limitations for uniaxial testing when testing soft materials; first, it may not be suitable when complex boundary conditions arise and is not possible to control the experimental condition entirely [23]. Second, these tests are inadequate to fully characterize the anisotropic behavior of these materials [7].

In a study made by Kanyanta and Ivankovic [16], the authors investigated the behavior of an ether-based polyurethane elastomer for the creation of mock arteries. Polyurethane was ideal for this application due to its high elasticity and resilience and adaptability to various shapes and sizes. Uniaxial tensile tests on dumbbell-shaped specimens were conducted, divided into three groups based on the strain rate.

For the low strain rate tensile tests ($< 1/\text{s}$), a standard Instron machine was utilized, as illustrated in Figure 1.1a. Intermediate strain rate tensile tests (between $1/\text{s}$ and $100/\text{s}$) were performed using a drop-weight tester (Fig. 1.1b). Load measurements were recorded with a calibrated strain gauge, with the zero position established at the striker and impact plate's initial contact point. High strain rate tests ($> 100/\text{s}$) were conducted with a split Hopkinson pressure bar in tension, as shown in Figure 1.1c. A swinging pendulum generated a tensile pulse, propagating along the bar into the specimen. Utilizing the transmitted and reflected strain signals and using the classical Kolsky analysis the specimen stress

$$\sigma(t) = E \frac{A_b}{A_s} \epsilon_t(t), \quad (1.1)$$

and the strain

$$\epsilon(t) = \frac{-2C_b}{l_s} \int_0^t \epsilon_r(t) dt, \quad (1.2)$$

were calculated. Here, A_b is bar's cross-sectional area, A_s the specimen's cross-sectional area, ϵ_t refers to the transmitted strain signal, ϵ_r is the reflected strain signal, l_s is the specimen gauge length, and C_b is the wave speed through the bar. Low strain rate tests were conducted under dry-room temperature, wet-room temperature, and wet at 37°C . Intermediate and high strain rate tests were performed exclusively under dry-room temperature conditions.

Test results demonstrated that ether-based polyurethane elastomer specimens were highly sensitive to temperature and humidity, as the material softened with increased levels of these factors. Young's modulus values for dry-room temperature setup 7.4 MPa, decreasing to 5.3 MPa and 4.7 MPa for the wet-room temperature and wet conditions, respectively. Moreover, the polyurethane exhibit varying Young's modulus values under dry-room temperature, depending on the elastomer's composition, with values ranging from 3.6 MPa to 14.8 MPa.

The material displayed minimal strain rate dependency at low strain rates, but exhibited moderate strain rate sensitivity at intermediate and high strain rates, where the Young's modulus ranged between 8 MPa and 12 MPa. However, for strains below 20 %, the outcomes showed repeatability across all strain rates tests.

For strain rates found in arteries around $< 2/\text{s}$, the variation of the Young's modulus was insignificant and this could be assumed to be constant. This study demonstrated that it is important to measure the properties of the elastomer under similar condition to the intended application, as properties varies under different conditions.

Uniaxial Compression Testing

Compression tests are also widely utilized to determine the stress-strain response and usually involve placing the specimen in between two plates and compressing the material (Fig. 1.2). The stress-strain response derived from this kind of testing serves in determining the deformation characteristics of the material including the fatigue and fracture resistance. Uniaxial compression tests may be affected by the interface friction between the specimen and the loading plates, leading to a nonhomogeneous deformation state, e.g., barrelling [3].



FIGURE 1.2: Uniaxial compression testing: Diagram of typical compression setup and influence of interface friction on the deformed specimen shape. Illustration is based on the "Mechanics of Solid Polymers" by Bergström [3].

Drass et al. [8] conducted a uniaxial compression test, showing that the lubrication was crucial for an homogenous stress and strain distribution. The specimen tested was made from Transparent Structural Silicone Adhesive (TSSA), a rubber-like material commonly used in laminated connections within glass structures. In this study homogeneous and inhomogeneous experiments were performed, as the goal was to determine an experimental setup, which ensured an homogeneous stress and strain distributions for the identification of material parameters [8].

The specimen was compressed with perfect slippage, where the plates and the specimen were lubricated before testing to ensure a frictionless support. A constant speed of $v_{UC} = 0.174 \text{ mm/min}$ was used for this test with a saBesto HHS 5000 machine. The compression test were conducted until a strain $\epsilon = 0.6$ was reached, as the standard deviation for large compression strain ($\epsilon > 0.5$) was too large. The test presented challenges in maintaining the lubrication throughout the test, as it tended to be pressed out between the test specimen and the pressure plates, resulting in increased friction.

The results of this experiment were processed to identify hyperelastic material parameters using standard fitting routines and inverse methods. The test suggested that only stress-strain response up to a strain value of $\epsilon = 0.5$ should be considered for the identification of the TSSA material parameters, as the friction's impact can be neglected for smaller strains.

In comparison, for a biomaterials, e.g., human soft tissues, a compressive testing of cartilage was conducted by Griffin et al. [12]. This study aimed to provide a protocol where compressive and tensile properties of human soft tissues can be evaluated and characterized with minimal destruction. By understanding these material's properties and calculating the Young's elastic modulus, it would be possible to obtain a benchmark for creating suitable tissue-engineered substitutes [12].

The mechanical response of cartilage is highly dependant to the fluid's flow through the tissue. The methods for compression testing can vary with confined or unconfined specimen, and the most prevalent, indentation (Fig. 1.3). In the unconfined compression the cartilage is pressured using a non-porous plate onto a non-porous chamber, leading to a predominantly radial fluid flow. For the confined compression the sample was placed in a sealed, fluid-filled impermeable chamber and loaded with a porous plate, making the fluid flow restricted to a vertical direction. Finally, the indentation testing employed a smaller indenter applied to the sample's surface perpendicularly, ensuring uniaxial compression and minimizing

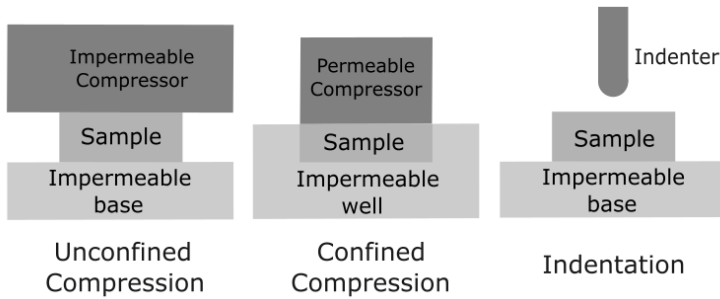


FIGURE 1.3: Uniaxial compression testing: Illustration of different compression methodologies for a cartilage specimen. Unconfined compression, confined compression and Indentation. Diagrams are based on the methodologies showed by Griffin et al. [12].

shear loading. All test were conducted in a hydrated environment and the cartilage was submerged in phosphate-buffered saline before and during the test to maintain the hydration. With the latest compression testing type it was possible to identify elastic and viscoelastic properties of the sample [12].

Indentation

Indentation testing, including micro and nanoindentation, is a popular method for characterizing the mechanical properties of soft materials [28]. One of the main advantages of indentation testing is that it requires minimal sample preparation and it is often a nondestructive technique, which allows the preservation of the geometry and tissue's architecture [24]. Furthermore, indentation is useful where more traditional testing techniques such as uniaxial or biaxial testing, are not possible to employ, and can also be utilized to evaluate nonlinear properties, e.g., viscoplastic responses[3].

Despite these advantages, there are some challenges when using indentation to characterize soft materials. First, a stress-strain response is difficult to obtain due to the complex boundary conditions, which introduces an inverse problem for the identification of material parameters [24]. Second, many of the current indentation configurations assume material isotropy, which may not be the case for biomaterials [9]. In addition, determining the mechanical properties of soft materials locally or at small scales is still difficult to achieve [30].

The usual indentation testing setup is shown in Figure 1.4, in this case a system applies a certain force to an attached indenter rod where and specific indenter tip. After the indenter tip goes to a determined displacement, it is possible to obtain a load-displacement curve. The deformation can be measured through an capacitance gauge or also optically, via laser measurements [3].

In a study made by

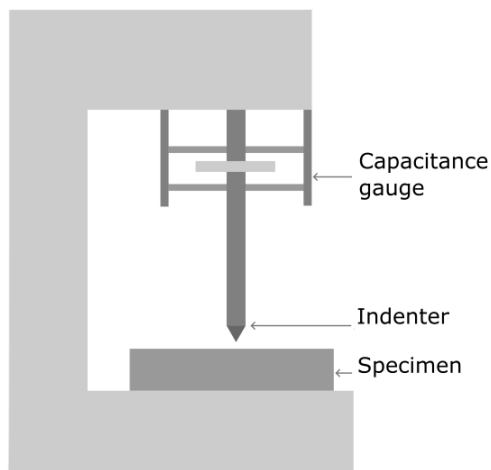


FIGURE 1.4: Nanoindentation experiment setup diagram with an indenter tip attached to a rod and a polymer as specimen. Diagram is based on the "Mechanics of Solid Polymers" by Bergström [3].

2 Experimental Model

The first phase of this project was to design and select an appropriate experimental model. This was essential to gather the necessary data from the tested material. This data will be used to determine the design parameters that can help to characterize the material's mechanical behavior.

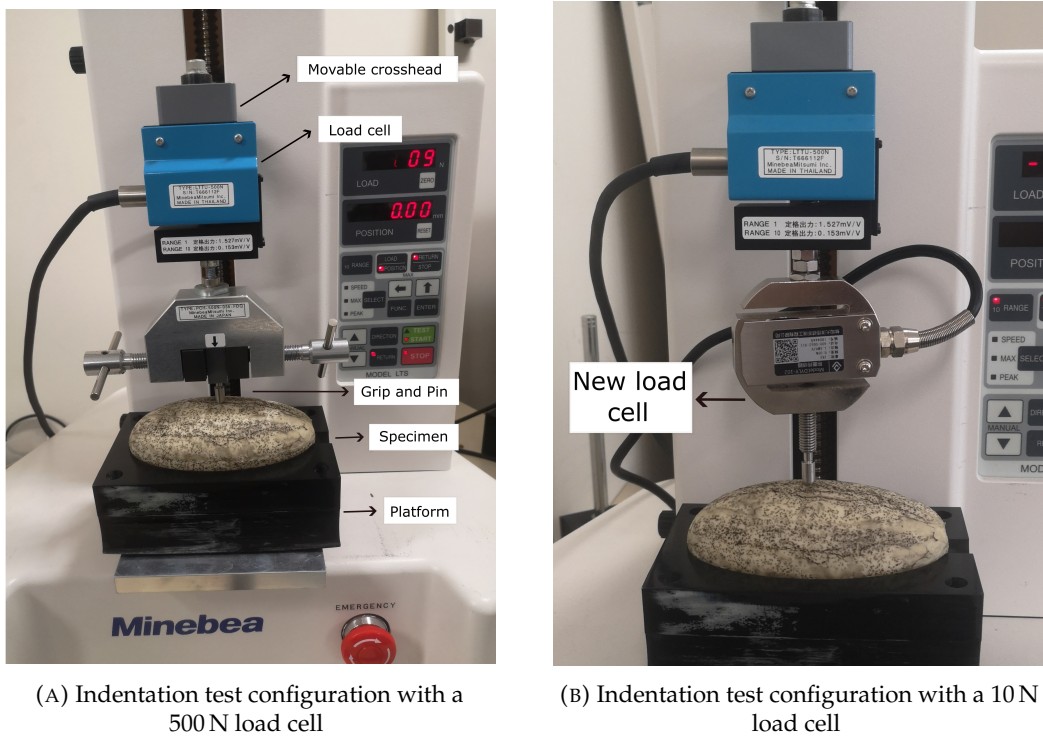
The experimental model I had the purpose of serving as a comparator for the experimental model II (see Section 2.2). At the beginning of the project, the desired experimental model to be analyzed was the second experimental model, which was developed and designed by Yokohama National University (YNU). As this second experimental model was still undergoing some improvements and corrections, a similar experiment was designed which could fulfill the same purpose.

The chosen experimental characterization for the inverse finite element method for the identification of material parameters for this project was indentation. The goal of these experiments was to observe the mechanical behavior of a soft material under compression using a rounded indenter. The aim was to determine the material behavior and observe the response under an indentation larger than the indenter radius. Additionally, by performing the indentation tests, the obtained data helped for a more in-depth understanding of the material's mechanical behavior for the chosen use cases and the determination of the main assumptions for the material modeling. The main advantage of indentation is the noninvasive feature, which will mostly become useful when a test sample should not be modified, e.g., an organ.

For both experimental setups, the specimen, which was tested, was made from a human skin gel. The human skin gel material was a two-component ultra-soft urethane resin. Polyurethane is widely used for biomedical applications, e.g., preparation of implants, wound dressings, artificial organs, and medical supplies.

Polyurethane can also be used for simulating organ tissues, as it can be tailored to mimic and match the mechanical properties of the desired biological tissues [27]. Furthermore, polyurethane can be synthesized to have a wide range of stiffness, elasticity, viscoelasticity, and can also be prepared with complex shapes for medical research purposes [15].

In this chapter, the different experimental models, which were used to evaluate the mechanical behavior of the ultra-soft polyurethane, will be described. In the first two subsections, will focus on the description and procedure of the experimental models, followed by explanation of the indentation test types. Consequently, an evaluation and analysis of the results will be provided and the main assumptions for the design of the material modeling will be defined.



(A) Indentation test configuration with a 500 N load cell

(B) Indentation test configuration with a 10 N load cell

FIGURE 2.1: First experimental model: Tensile and compression machine with an indenter with a rounded head. Test Specimen made from ultra-soft polyurethane resin positioned on a fixed platform with a similar shape for constraint.

2.1 Experimental Model I

Description of the Experimental Setup

The first indentation test configuration was done by adapting a tensile and compression testing machine, model LTS - 500 NB from MinebeaMitsumi.Inc (Fig. 2.1). This machine possess a maximum load capacity of 500 N, and test speeds of 10 mm/min, 20 mm/min, 30 mm/min. To achieve an indentation testing configuration, a pin was attached to the movable crosshead holding grip, as shown in Fig 2.1a. The indenter had a rounded head made of stainless steel with a radius of $r_{i1} = 3$ mm and a length of $l_{i1} = 11$ mm.

The specimen possesses a ellipsoidal form with with a minor radius $r_1 = 35$ mm and a major radius $r_2 = 60$ mm. This specimen geometry is supposed to simulate a kidney with an extracted tumor; therefore, on the lower part of the specimen a half ellipsoid with a minor radius $r_{t1} = 10$ mm and a major radius $r_{t2} = 15$ mm was removed (Fig. 2.2). The specimen was prepared by a YNU laboratory member, by 3D printing a mold with the wanted dimensions and a ellipsoidal shape, and filling it with liquid resin. Additionally, it was left to cure for around 30 h. It is relevant to clarify, that this sample had been created months before the development of this experimental setup and had been utilized in other projects conducted from the laboratory. This available specimen was positioned on a platform fixed to the base, which suited the ellipsoidal geometry for properly constraint.

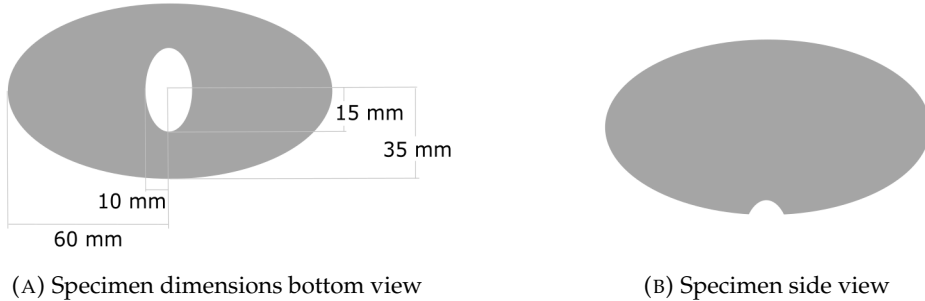


FIGURE 2.2: First experimental model: Specimen dimensions made from ultra-soft polyurethane resin for indentation test.

Procedure for Conducting the Experiment

For the indentation test after placing the specimen on the platform, the indenter was positioned slightly on the surface of the point of interest. The test was conducted with a room temperature of approximately 22 °C. To perform the test the indenter was then lowered onto the surface of the specimen at a velocity of 10 mm/min. The indentation depth was controlled by limiting the maximum depth, and the test stopped once the inserted depth was reached. The indenter returned to its original position after reaching the maximum depth with a rate of 100 mm/min. Due to the material properties, the specimen returned to its original shape. The result of the indentation test was a load-displacement data, which was recorded with a sampling rate of 63 Hz using a load cell of ± 500 N and a encoder to measure the displacement.

The measurement accuracy according to the specification of the machine, has a relative reading error of 1.0 %. The indentation test was repeated five times on the same sample to ensure and observe reliability and repeatability. Furthermore, the raw data collected from the test was processed and analyzed using Excel.

During the initial indentation test using the 500 N load cell, the collected experimental data showed noise that could affect the accuracy and reliability of the results. The noise was likely caused by sensitivity of the lead cell. The ultra-soft polyurethane material showed force readings, which were near the lower limit of the load cell's range, which adding any other external factors, results in noisy measurements. To address this issue, a load cell of 10 N was installed (Fig. 2.1b). This change improved the quality of the measurements and reduced the noise in the data. The change to the load cell had some implication to the experimental setup, such as removing the holding grip, and designing a part which could connect the indenter with the new load cell. In addition to changing the load cell, a simple filtering method was used to improve the experimental data. After applying the filter, the noise in the data was reduced, resulting in more smoother force reaction readings.

The applications of the combinations helped to improved the quality and accuracy of the data and gave important information about possible measurement errors to take into consideration for of the experimental model designed by YNU. At last, The filtered data was used for subsequent analysis and interpretation for the inverse finite element method approach for the material parameter identification.

2.2 Experimental Model II

The second experimental model was developed and designed by Yuta Mori, a member of the Yamada Laboratory from the Mechanical Engineering department of Yokohama National University. The main aim for this experimental method was to be able to identify the physical properties of organs in a state that closely resembles the *in vivo* environment. Additionally, this model sought to achieve two objectives: firstly, to develop a loading system to acquire the data required for an inverse analysis, and secondly, to establish a measurement process in case of a total nephrectomy [20].

Furthermore, for the present experimental setup a new sample was prepared using the same material as the previous one, i.e., human skin gel made from ultra-soft polyurethane resin, and following the same manufacturing process as described in Section 2.1.

The resulting data from the experimental model served for the basis of the material parameter identification for the inverse finite element method approach. The processed data obtained from this experimental model assisted in the calibration and assessment of the design parameters employed in the validation for the computational model.

Description and Procedure of the Experimental Setup

In this experimental model the indentation loading system, which gathers data of the indentation depth, reaction force and general deformation. The experimental device consists of a 6-axis force sensor, a laser displacement transducer, and 3D cameras placed in four directions to obtain the point cloud data based on the coordinate system of each camera. Fig.2.3 shows the setup of the experiment. For our project, the 6-axis force sensor and the laser displacement were mainly used. The loading system is operated by specifying the movement of the loading rod in advance, and the indentation is performed in the direction normal to the contact surface to prevent slippage (Fig. 2.4).

The specimen, same as in the first experimental model (Section 2.1), possessed the same dimensions, a minor radius $r_1 = 35$ mm and a major radius $r_2 = 60$ mm, and was made from ultra-soft polyurethane resin. Consequently, the platform is also bowl-shaped. For this experiment, the platform base was made from transparent acrylic resin to record the contact status of the bottom surface [20]. The maximum load capacity of the load cell is 200 N and a theoretical force resolution of 0.001 N. In addition, the resolution of the laser displacement sensor is 0.05 mm. The indenter is sphere-shaped with a radius of $r_{i2} = 3$ mm and was made from ruby with the following specifications; a Young's Modulus of $E_{i2} = 440$ GPa and a Poisson's ratio of $\nu_{i2} = 0.3$ mm.

The indentation test was conducted under room temperature conditions. Also, the sample was placed on acrylic platform and the indenter was lowered at constant velocity of 30 mm/min. The experiments were conducted for each loading point five times on the same sample, and the average of the results were calculated.

Furthermore, to minimize the friction during the indentation process, the indenter and the loading surface on the specimen were covered with a thin layer of lotion. This was done due to inaccuracies and step-like data shown in the measurements. Therefore, to reduce this measurement error, the application of lubricant was

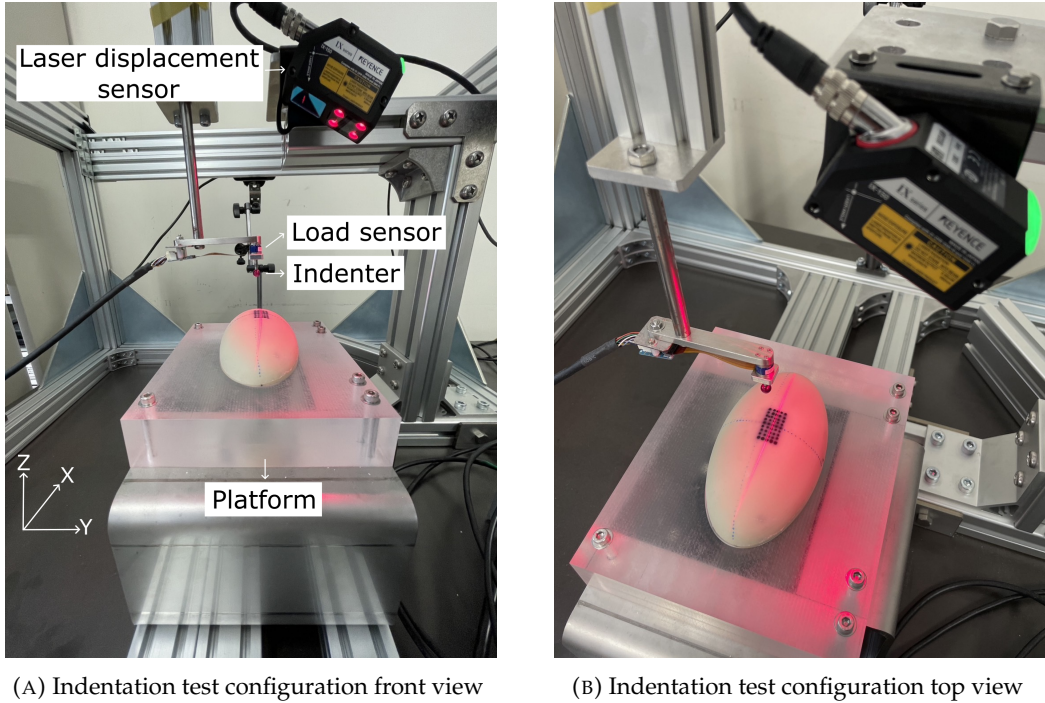


FIGURE 2.3: YNU experimental model: 6-axis sensor Test Specimen made from ultra-soft polyurethane resin positioned on a fixed platform with a similar shape for constraint.

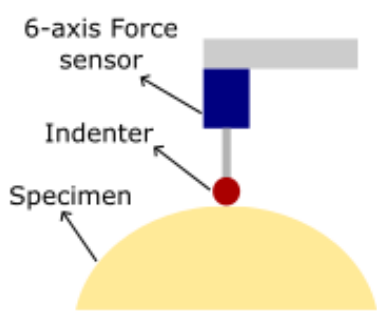


FIGURE 2.4: YNU experimental model: Loading diagram showing initial position of the indenter in normal position [20].

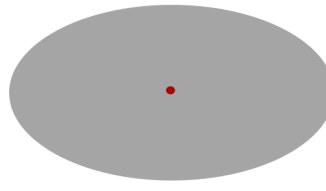


FIGURE 2.5: Middle test point: Loading point (Red point) on the top surface of the specimen.

employed, ensuring a smoother and more controlled indentation process. Finally, the data was also processed and assessed using Excel.

Analysis and Comparison of Experimental Techniques

The second experimental model offers some advantages over the first model. Firstly, it enables not only the measurement of the total force reaction, but also the analysis of the force reaction components F_x , F_y and F_z . This allows for a better understanding of the material's mechanical behavior, as it allows the identification of a specific contribution of the force components and it contributes to identify other mechanisms such as viscoelasticity, plasticity, and creep. In addition, the second model allowed for the measurement of the deformation in other points near the tested loading point. This provides additional information of the material parameters, as it facilitates the characterization of the deformation behavior beyond the direct vicinity of the indentation point. Furthermore, only this test configuration makes use of a lubricant, as this experimental setup could show some inaccuracies in the first data sample.

In contrast, the first experimental model only measures the total force reaction against the indentation depth, without providing any information about the contribution of each component. While the first model allows the data gathering in simpler and more straightforward way, it may not capture the whole complexity of the material.

2.3 Experimental Tests Description

Middle Point(MP)

The first use case for the indentation test was performed at the midpoint of the major and minor axis of the ellipsoid (Fig. 2.5). This point was selected to ensure that the indentation was normal to the surface, thereby avoiding the influence of potential shear forces which could influence the measurements.

Additionally, the first indentation depth was chosen arbitrarily, for the first experimental model was $h_I = 3.8$ mm, and for the second experimental model was $h_{II} = 4$ mm. This depth was considered to be an appropriate compromise that would allow to capture the nonlinear behavior of the material, while also remaining a simple use case to reproduce in a computational model in ANSYS.

As the main objective is to find a path, which lets identify the material parameters, the most basic use case was selected and from this point the complexity was gradually built on. Through this approach, it was possible to establish a solid foundation for the subsequent experiments and data analysis.

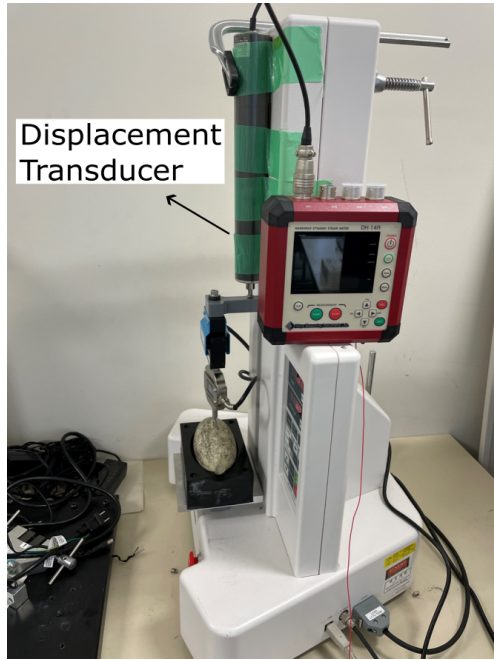


FIGURE 2.6: Load-Unload Case: Experimental model I with modified configuration setup, on top of the movable crosshead a displacement transducer was equipped to capture unloading data.

Load-Unloading (LU)

Building on the previous test point (Fig. 2.5), an indentation test was conducted on the same point, with an indentation depth of 4 mm, but this time in a loading-unloading case.

The first experimental model setup, as described in Section 2.1, was unable to measure the displacement and force reaction during the unloading of the specimen. As a result, certain modifications were made to the experimental setup. Due to time constraints, the modification of experimental model I (EPI) was also executed by laboratory members Mori Yuta in YNU. To capture the displacement and force reaction during the unloading, a displacement transducer was equipped to the tensile and compression machine as shown in Figure 2.6.

The aim of this use case, was the observation of a possible hysteresis behavior, as well as to investigate the viscoelastic properties of the material. The load-unload test was performed at six different loading speeds, namely, 10 mm/min, 20 mm/min, 30 mm/min, 50 mm/min on the same specimen. Each speed configuration was repeated five times, and the results were averaged to reduce the effects of experimental variability.

The load-unload case helped to determine whether complex material behavior such as viscoelasticity, could be neglected for the computational model of the middle point test. The results of this experiment were used to make this decision, which has important implications for the simplification of the computational model and its accuracy and reliability.

Nearby Point (NBP)

In addition to the indentation performed on the middle point of the surface, further indentations were conducted on nearby points. From these indentation tests,

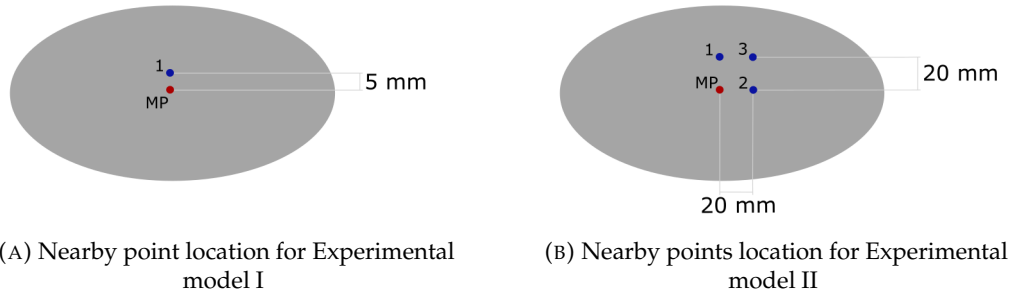


FIGURE 2.7: Nearby test point: Loading points for each experimental model to analyze shear stresses and to validate employed for the validation of the computation models.

force-displacement curves were recorded. For each indentation the same experiment configuration, e.g., indentation depth and indentation speed, was employed as described in Sections 2.1 and 2.2.

For the first experimental model, only one nearby point located $p_{I1} = 5 \text{ mm}$ to the right of the middle point was selected as shown in Figure 2.7a.

For the second experimental model, three additional nearby points were tested. These points were located at distance of $p_{II1} = 20 \text{ mm}$ to the right, $p_{II2} = 20 \text{ mm}$ downwards, and a third point $p_{II3} = 28.3 \text{ mm}$ diagonally from the middle point forming a square (Fig. 2.7b).

The objective of these testing points was to gain a deeper understanding of the effect of the shear stresses on the indentation response. Furthermore, the results of these points allowed for the validation of the computational model and the selected material model.

2.4 Analysis and Overview of the Data and Results

In this section, the results of the experimental models described in the previous sections will be presented and analyzed. The objective is to understand the behavior of this ultra-soft polyurethane material under indentation and establish the first assumptions for the development of the computational model, as well as the material model. The section will start with a brief summary of the tests, followed by the analysis of the force-stroke curves gathered throughout the experiments.

The experimental model I served mainly as a comparator and a quick way to gain an idea of the mechanical behavior under indentation, for this model three different use cases were measured. An indentation in the middle point of the surface with an indentation depth of $h_I = 3.8 \text{ mm}$. Subsequently, the load-unload case was observed under an indentation depth of $h_{I2} = 4 \text{ mm}$, and with six different speeds ranging from 10 mm/min to 100 mm/min . Finally, a nearby point was selected near the middle point, $p_{I1} = 5 \text{ mm}$ to the right, to use it as a validation point for the selected material model.

A similar process was followed for the experimental model II (EPII), the middle point indentation was performed with an indentation depth of $h_{II} = 4 \text{ mm}$ and a indentation speed of 30 mm/min , where the force components could be observed. Similarly, the load-unload scenario was tested under the same conditions, and three nearby points were measured.

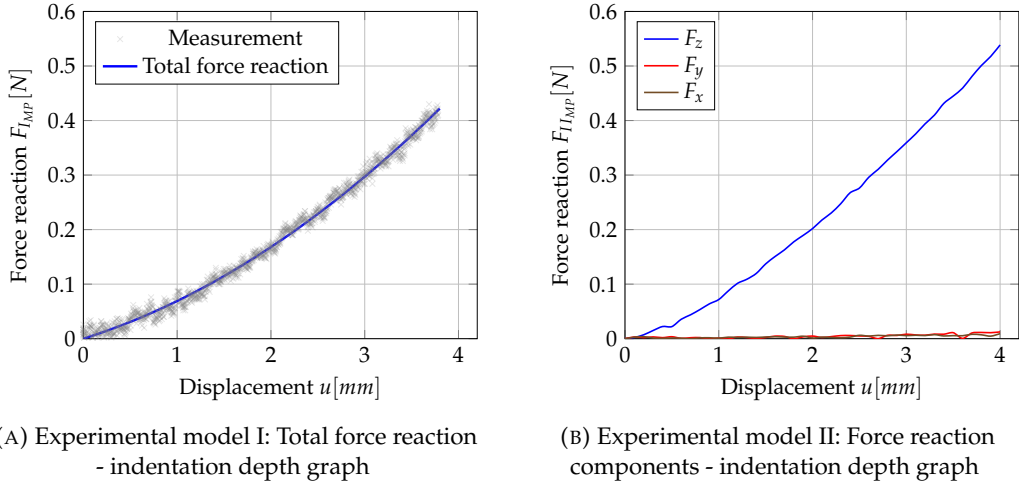


FIGURE 2.8: Load-displacement curve experimental data for Middle Point use case for both experimental models.

2.4.1 Middle Point

The results of the indentation test at the middle point for both experimental showed a clear nonlinear behavior. It is assumed that this material possess a elastic-plastic behavior, which in a typical load-displacement curves has four known stages [11]:

1. Nonlinear elastic (self-adjusting): In this stage, the material adjusts itself to the loading conditions, and the deformation is elastic and reversible.
2. Linear elastic: The material is bearing the external load in this stage, the deformation is still elastic and reversible
3. Nonlinear plastic (failing): With the increase of the external load, the material reaches its yield point and undergoes permanent deformation
4. Failure: The material fails leading to permanent damage.

Figure 2.8 shows the results of the two indentations at the middle point of the specimen surface. The load-displacement curves showed nearly identical material behavior for both experimental configurations. This use case demonstrate the nonlinear-elastic behavior of the material, as there was no evidence of a yield point or plastic behavior. Both curves began at zero, and the force increased gradually with increasing, resulting in a slightly concave shape.

Figure 2.8a displays all the measurements points obtained from experimental model I and its polynomial approximation. This approximation was used for the subsequent steps of the iFEM approach. The maximum total force for experimental model I at a maximum indentation depth of $u_{I,MP} = 3.8$ mm was $F_{I,MP} = 0.4218$ N. For experimental model II, at an indentation depth of $u_{II,MP} = 4$ mm, the maximum forces for each component were $F_{Z,II,MP} = 0.546$ N, $F_{Y,II,MP} = 0.0124$ N, and $F_{X,II,MP} = 0.0093$ N.

From load-displacement curve of experimental model II (Fig. 2.8b) it was evident that the force reactions in the X and Y directions could be disregard, as these were considerably lower than the force reaction in Z direction. Therefore, the focus in further analysis was mainly on the force reaction in Z direction. Additionally, this

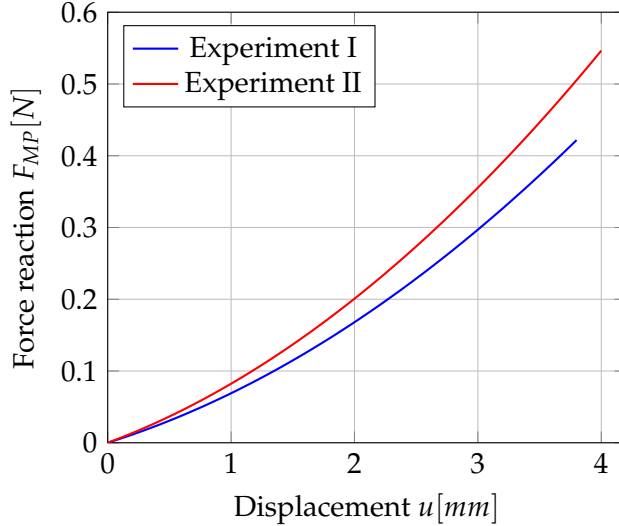


FIGURE 2.9: Total Force Reaction-Displacement curve: Comparison between experimental data for Middle Point use case from both models.

case revealed that shear stresses were minimal, which is consistent with the purpose on performing the indentation with the least influence of external factors.

Figure 2.9, shows that the load-displacement curve of experimental model I has a similar initial behavior to that of experimental model II. However, as the indentation depth increases, the curve of experimental model I is positioned lower than that of the second model. One possible explanation for this difference could be the effect of aging on the material properties of the specimen used in the first model. Since the specimen used in this configuration was manufactured months before (Section 2.1), it is possible that the aging had led to a decrease in its mechanical properties, resulting in a lower resistance to deformation and therefore, lower stiffness than the newly manufactured sample. Another possible explanation could be the presence of external factors during the conduction of the experiments or the configuration of these. Nevertheless, as the main purpose of this Middle Point use case was to minimize the influence of these factors, this explanation seems less probable.

2.4.2 Load-Unloading

Following the Middle Point use case, in addition to the loading data, the unloading was also captured for both experiments as explained in Section 2.3. Figure 2.10 shows the load-displacement curve for experimental model I and next to it experimental model II. Both results exhibited during the unloading some degree of hysteresis, as there was a slight difference in the force reaction measured. However, the material displayed good elastic behavior, as it returned to its original shape once the indenter was removed.

The hysteresis displayed for both configurations could have occurred due to several reasons, such as viscoelastic behavior of the material, or external factors, like friction between the indenter and the specimen, surface roughness of the indenter,

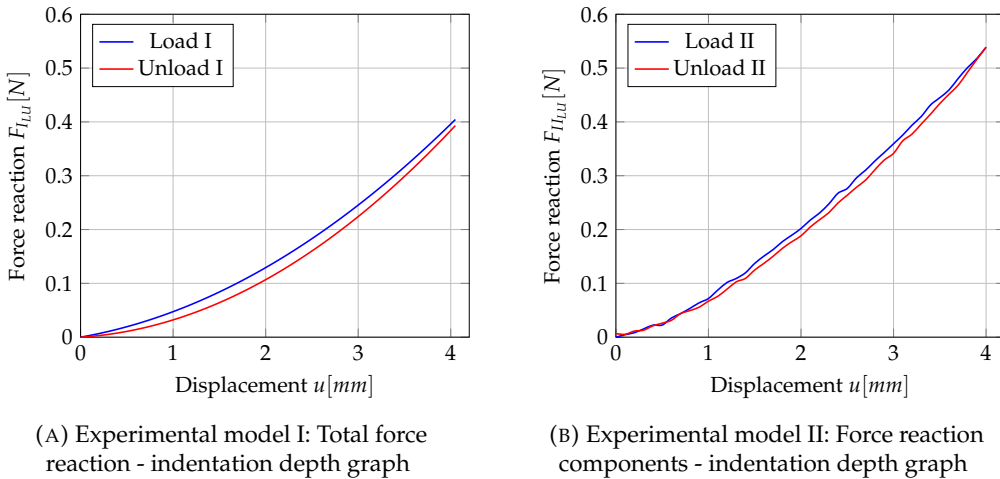


FIGURE 2.10: Load-displacement curve experimental data for Load-Unload use case for both experimental models.

test configuration, and so on. To examine closer the main reason for the hysteresis, only with first experimental setup, a series of indentations tests were performed with different speeds.

Figure 2.11 shows the result of the load-unload indentation tests from the lowest to highest value for the indentation speed. It could be observed, that the curves exhibit a similar material behavior. A slight increase in the hysteresis was observed when the indentation speed was increased. Specifically, during the loading, the force reaction were slightly higher as the speed and indentation depth increased. During the unloading, the only notable difference was observed with 100 mm/min, where the unloading curve had the lowest values.

From the results and in the case of ultra-soft polyurethane, it is likely that the hysteresis is primarily due to the viscoelastic behavior of the material. Nevertheless, for the tests done in the middle of the surface, it was decided that the viscoelastic properties could be neglected for the material modeling seeing that the difference between the curves is not impactful for the first stage of the identification of the material parameters.

2.4.3 Nearby Point

To complement the analysis of the viscoelastic behavior of the material, a nearby point located $p_{11} = 5$ mm to the side of the midpoint, following the minor axis of the ellipsoid (see Subsection 2.3). This location was chosen to investigate if the mechanical response of the material is uniform across the surface and if any variations could be detected within a short distance. Figure 2.12 shows the results of the Middle Point use case vs. the selected Nearby Point case for experimental model I.

The new load-displacement shows nearly identical behavior to that of the first case, except for the last part of the curve, where the Nearby Point curve goes slightly lower. The maximum force obtained for the Nearby Point case was $F_{I,NBP} = 0.4134$ N, which is lower than the one obtained before, which was $F_{I,MP} = 0.4218$ N.

It can be concluded, that the results from this nearby point support the findings from the Middle point test, indicating that the material behavior was homogeneous in the region of interest. The small difference in the maximum force values could

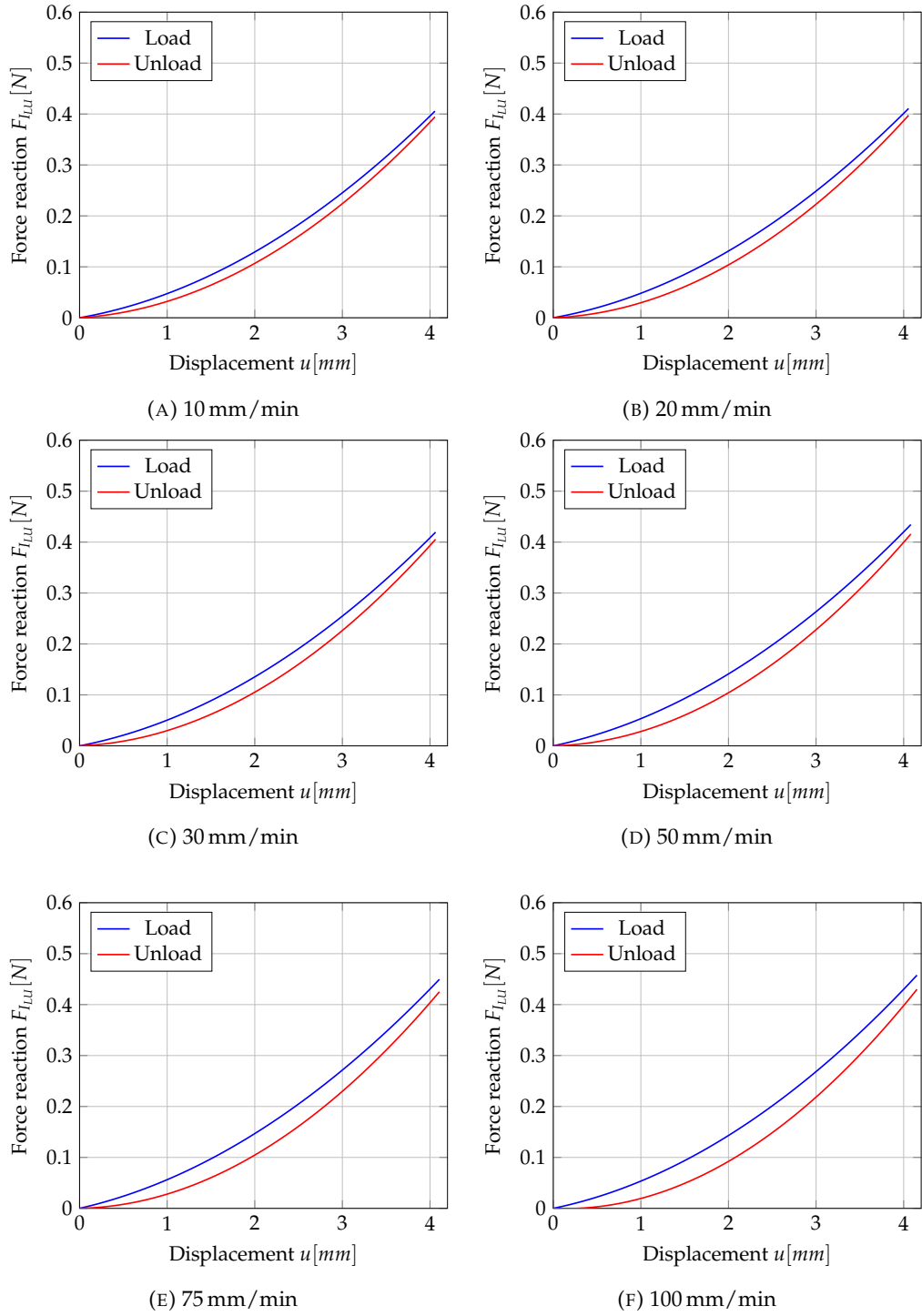


FIGURE 2.11: Load-Unload Use Case: Analysis of Viscoelastic material properties by using six different indentation speeds. Load-Displacement curves were obtained from the first experimental test configuration.

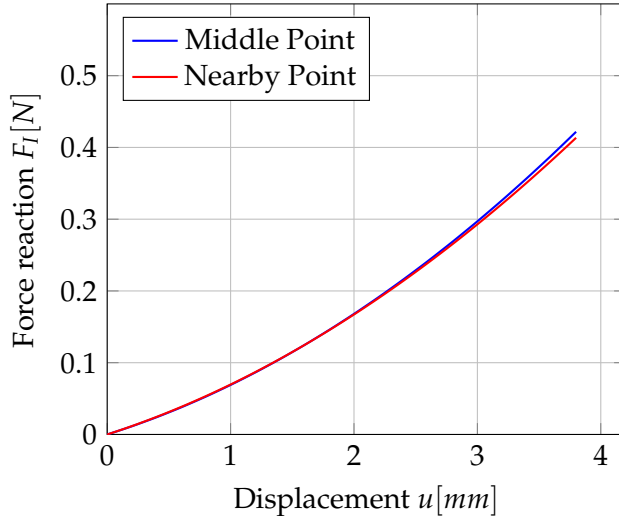


FIGURE 2.12: Total Force Reaction-Displacement curve: Comparison between experimental data for Middle Point and Nearby Point. This point was located 5 mm right from the midpoint, following the minor axis of the ellipsoid.

be due to the variations in the experimental conditions, e.g. the increment of the gradient of the contact surface due to the curvature of the specimen. This change could potentially affect the distribution of the stress and strains within the material. Nonetheless, these differences were not significant enough to affect the overall conclusions.

With the measurements taken in the additional nearby points for experimental model II (Subsection 2.3), it was possible to investigate whether the small variations in the results obtained with experimental model I could be attributed to the difference in the gradient of the contact surface. Figure 2.13 shows the result for each force reaction component for all four tested points. In X-direction, the maximum force was observed for point 2, which had the smallest gradient contact surface, followed by point 3. These points were 20 mm down along the X-axis, in contrast to the other two points, which were at the origin of the X-axis. For the middle point and point 1, which had the largest contact surface gradient, the X-component force reaction was almost 0 N.

Similarly, in Y-direction, the maximum force was observed for point 3, followed closely by point 1. For the middle point and point 2 the Y-component force reaction was almost 0 N. Point 3 and point 1 were 20 mm right along the Y-axis, and the middle point and point 2 were at the origin of the Y-axis. As for the Z-direction, the maximum force was observed at the middle point, followed by point 2, and consequently with similar results point 1 and point 3. For all the points the results in Z-direction are more significant than in the other directions.

These results suggested that variation in the gradient of the contact surface may have contributed to the small differences in the results obtained with experimental model I. Specifically, it was observed, that with a smaller contact surface gradient the higher the X-component the same for the Y-component with the larger contact surface gradient. In conclusion it is possible to confirm that the material behavior was homogeneous, and that the larger the contact surface gradient became, the lower the

total force reaction.

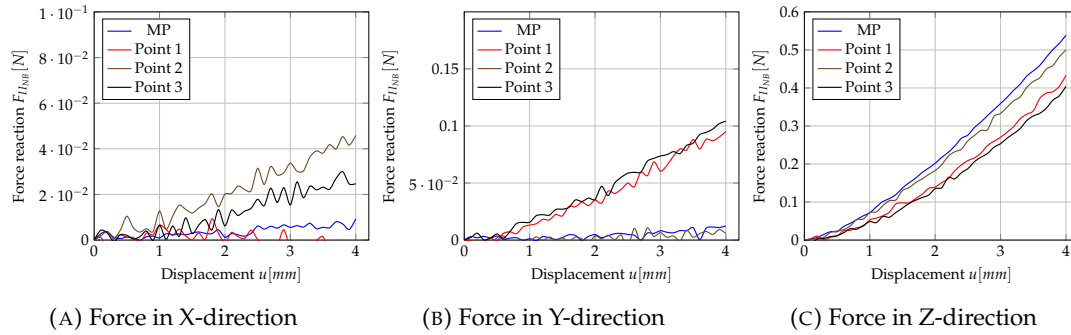


FIGURE 2.13: Nearby Point Use Case: Analysis of shear stresses by observing three different nearby points on the specimens surface. Load-Displacement curves were gathered from Experimental Model II showing each force component.

2.5 Main Assumptions for Material Modeling

In this section, the main assumptions based on the results obtained from the indentation tests will be summarized. These assumptions will be used for the development of the material models. As previously mentioned, one of the goals of this project was to develop the material model from an ideal scenario, while considering the limitations at each level. The complexity of the material model was incrementally increased until a set of material parameters that provided a proper compromise to the experimental results was obtained. Defining these levels allowed the assessment of the impact of each parameter on the development of the material model.

Based on the presented experimental data and previous discussion, the following assumptions could be made:

1. The material can be assumed to be homogeneous in the region of interest for the Middle Point Case, as the results from the nearby points support the findings from midpoint test.
2. Nonlinear elasticity is observed and hysteresis can be neglected, as the changes observed with the different loading speeds were not significant enough to affect the initial results.
3. The viscoelasticity of the material can be ignored for the first design of the material model, as the material returns to its original shape and almost no energy is lost during deformation.
4. Friction and shear stresses will be neglected, as in the Middle Point case the observed force components in x and y directions are non-relevant.

It is important to mention, that it was noted that the main assumptions made may not hold for different experiment settings, such as higher loads, longer loading times, higher temperatures, high shear stresses, and so on. Therefore, it was important to keep these assumptions in mind when using the chosen material model in a validation case.

2.5.1 Level 1: Linear elasticity

The first level a linear elastic model was used. This model assumed that the material behaves linearly, i.e., the deformation is linearly proportional to the applied load and the material returns to its original shape after the load is removed. This model is based on Hooke's law, where the stress-strain relationship is

$$\sigma = E\varepsilon, \quad (2.1)$$

where σ is the stress, E is the elastic modulus, and ε is the strain. For the Middle Point Case, the material is assumed homogeneous and isotropic, thus the elastic modulus is the same in all directions. For an indenter with a spherical tip, the contact area A between the indenter and the specimen can be approximated as,

$$A = r_i^{\frac{1}{2}} h^{\frac{1}{2}}, \quad (2.2)$$

where r_i is the radius of the indenter, and h is the indentation depth. For a spherical indentation assuming the Hertzian contact theory, the Hertzian relationship between the applied force F and the indentation depth h is [18],

$$F = \frac{4Er_i^{\frac{1}{2}}h^{\frac{3}{2}}}{3(1-\nu^2)}, \quad (2.3)$$

where E and ν are the Young's modulus and Poisson's ratio of the indented material. This Hertzian relationship is used as the analytical basis on the contact of ellipsoid bodies in indentation experiments [18]. This model provided a simple and straightforward approach to describe the material behavior under small deformations. The elastic modulus and the Poisson's ratio are the two main parameters that will be used for this model. Additionally it was assumed that the material is near incompressible, therefore, a fixed Poisson's ratio was chosen,

$$\nu = 0.49, \quad (2.4)$$

leaving the analysis of one parameter, the elastic modulus. The linear elastic model served as a basis for the more complex material models developed in the subsequent levels, and it provided a reference point for the identification of other material parameters.

2.5.2 Level 2: Hyperelasticity

The second level introduces a higher complexity, as more material parameters are analyzed. For this level a Neo-Hookean model was used to describe the material behavior based in the strain energy potential function. The elastic strain energy potential function for the Neo-Hookean material model is given by

$$W = C_1(I_1 - 3) + \frac{1}{D_1}(J - 1)^2, \quad (2.5)$$

where C_1 is a material constant, D_1 the material incompressibility parameter, J the determinant of the elastic deformation gradient, and I_1 is the first invariant of the right Cauchy-Green deformation tensor, i.e.

$$I_1 = \lambda_1^2 + \lambda_2^2 + \lambda_3^2, \quad (2.6)$$

where λ are the principal stretches [21]. To maintain conformity with linear elasticity, the material constant

$$C_1 = \frac{\mu}{2}, \quad (2.7)$$

where μ is the shear modulus or the second Lamé parameter. If the material is assumed to be incompressible,

$$J = 1, \quad (2.8)$$

and the second term in the strain energy potential W becomes zero [22].

The Neo-Hookean model requires two main parameters to be identified; the shear modulus μ and the incompressibility parameter D_1 . The incompressibility parameter relationship with the initial bulk modulus

$$K = \frac{2}{D_1}, \quad (2.9)$$

can be defined [2]. The relationship between the shear modulus, the elastic modulus, and the Poisson's ratio

$$\mu = \frac{E}{2(1 + \nu)}, \quad (2.10)$$

can be calculated, as well as for the bulk modulus

$$K = \frac{E}{3(1 - 2\nu)}. \quad (2.11)$$

Using the results of the first level with E and ν it is possible to establish a possible range for μ and D_1 . This targeted range helped in the reduction of computational time for simulations. The hyperelastic model provides a more accurate description of the material behavior in comparison to linear elastic model, as this model takes into account the nonlinear behavior of the material.

3 Computational model

3.1 Middle point

3.1.1 Description

The quasi static nature of the indentation experiment allows the use of a static structural analysis.

For the creation of the computational model, the SOLID 187 elements were used. The mesh for the whole model is formed from quad tetrahedral elements. The platform and the specimen have a global element size of 5 mm. The indenter has an element size of 0.5 mm. In the area of the indentation, there is finer mesh with an element size of 1 mm and a radius of 8 mm.

3.1.2 Analysis and Complications

There are two main factors which increase the complexity of the validation of the simulation and those are, the contact nonlinearity, and the element distortion due to indentation experiment. These issues make the computational time expensive, as it requires manual solutions for the meshing in the area of importance, and small time steps. For that, the nonlinear adaptive meshing option in ANSYS Workbench was applied, which does a remeshing process if a certain parameter is exceeded. Specially, for larger indentation cases, this option shows a more stable model with a good mesh convergence analysis.

A force-displacement curve, shown in Fig... is generated from the first assumption, for this case

For both cases

3.1.3 Verification of the Simulation Model

Mesh Convergence Analysis

Platform vs Fixed Support

3.2 Nearby point

4 Inverse Finite Element Method for Material Parameter Identification

4.1 Procedure of IFEM

4.2 Material Modeling

In an ideal and first scenario, this material can be assumed as linear, isotropic, elastic and nearly incompressible. For this case, there are two main variables, the Young's Modulus E , and the Poisson's ratio ν .

From the parametric analysis, it is possible to see that the bulk modulus of this material does not possess a big impact in the FE simulation results. This conclusion combined with the results from the Poisson ratio in the first material model coincide with the statements from Bergström, where it is no vital to know these parameters to obtain accurate FE computational models, as these have limited influence on the mechanical response. [3]

4.2.1 Response Surface Optimization

Linear Elastic Model

Hyperelastic Model: Neo-Hookean

4.2.2 Objective Function Optimization

4.2.3 Analysis and Comparison of Each Approach

5 Results

5.1 Overview and Analysis

5.2 Framework proposal

5.3 Verification and Validation

5.3.1 Deeper indentation

5.3.2 Deformation profile analysis

5.4 Limitations and implications of the results

5.4.1 First Experimental model

The chosen experimental technique for the inverse identification for this project was indentation. The test specimen used for this experiment was a ultra-soft polyurethane resin. As shown in Fig.. the specimen possesses a ellipsoidal form with with a minor radius $r_1 = 35$ mm and a major radius $r_2 = 60$ mm. This was positioned on a fixed platform that suited the ellipsoidal geometry of the specimen to constrain its movement. The specimen was tested in a indentation test configuration with a tensile/compression machine. To achieve this congiguration a pin with a rounded head made of structural steel, with a radius of $r_3 = 3$ mm was attached to the holding grips followed by a force load cell. The result of indentation test was a load-displacement points. The approximated polynomial curve was used as a reference for the material modeling.

The measured force reation F_1 data showed a very small number, so the first 50 N load cell displayed a lot of noise in the measurements. Therefore, the load cell was change to 10N to reduce this interference. The 10 N load cell displayed the force-displacement curve of the indenter and the specimen in a finer way. Furthermore, in order to get the measurement of the load and unloading process of the indentation a displacement sensor was attached to the tensile machine.

The indentation depth h_1 selected for the first model was 3,8 mm on the middle of the top surface of the specimen. This indentation depth surpasses the pin radius r_3 and was chose arbitriarily to analyze the behavior of the material on the defined position. Additionally, it was observed that in soft materials it is easier to capture some parameters with a larger indentation. Some references also observe that with indentation depth lower than indenter radius has a lot of noise and do not describe th results accurately.

From the first experimental model we can observe that the material shows a non-linear behavior and the maximum total force reaction F_1 lies around 0.45 N. Furthermore, when applying different speeds, as show in Fig. it is also possible to observe that the hysteresis increases. This increasement shows that the material possesses a viscoelastic behavior, however as this increasement is not significantly, it is possible to neglect viscoelasticity for the first stages of the project.

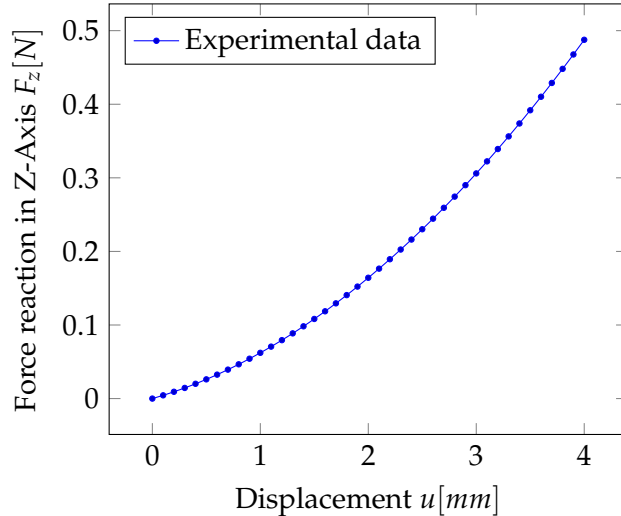


FIGURE 5.1: Experimental Load-displacement curve.

5.4.2 Second Experimental model

The second experimental model was developed by Yokohama National University. Similar to the first experimental model the test specimen and the platform were it lies, has the same dimensions, minor radius $r_1 = 35$ mm and a major radius r_2 of 60 mm. The test specimen is also made from the same material, ultra-soft polyurethane resin.

The indenter on the other hand, is a sphere made of ruby, the sphere radius is also equal to the radius of the pin r_s 3 mm and attached to it, is the force load cell.

A laser is used to measure the displacement which results in a load-displacement curve. With this model it is possible to not only determine the total force reaction, but also its components F_x , F_y and F_z . Furthermore, with the laser it is also possible to observe the deformation not only in one point but around the whole area. This allows as to analyze the deformation of the whole structure.

The indentation speed selected was and with an indentation depth of h_s is 4 mm. With this experiment, 4 key points on the specimen's surface were chosen: First, in the middle and three other points, one to right, one down, and one diagonal to middle, forming a square with a distance between points of d_s 20 mm.

Similar to the previous model, Fig. shows a nonlinear behavior with a maximum force reac

5.5 Material model framework assumptions

The first point to be analyzed, which is used to build a material model is point No. 1, in the middle of the surface. The advantages from this case, is the less influence of external factors. For this case it is viable to assume, that shear stresses can be neglected and offers a simple model to focus on the material definition.

For this project, there is a focus on the limitation of each material model, departing from an ideal scenario. From this point on the material will be built accordingly and for each model the influence of the material parameters is going to be assessed.

5.5.1 First Material model

Linear elasticity

Hyperelasticity

The strain energy density function for the Neo-Hookean material model is given with

$$\Psi = C_1(I_1 - 3),$$

where C_1 is a material constant and I_1 is the first invariant of the right Cauchy-Green tensor. Neo Hookean and Mooney Rivlin comparison

5.6 Computational model

The quasi static nature of the indentation experiment allows the use of a static structural analysis.

For the creation of the computational model, the SOLID 187 elements were used. The mesh for the whole model is formed from quad tetrahedral elements. The platform and the specimen have a global element size of 5 mm. The indenter has an element size of 0.5 mm. In the area of the indentation, there is finer mesh with an element size of 1 mm and a radius of 8 mm.

There are two main factors which increases the complexity of the validation of the simulation and those are, the contact nonlinearity, and the element distortion due to indentation experiment. These issues make the computational time expensive, as it requires manual solutions for the meshing in the area of importance, and small time steps. For that, the nonlinear adaptive meshing option in ANSYS Workbench was applied, which does a remeshing process if a certain parameter is exceeded. Specially, for larger indentation cases, this option shows a more stable model with a good mesh convergence analysis.

A force-displacement curve, shown in Fig... is generated from the first assumption, for this case

For both cases

5.7 Material model

In an ideal and first scenario, this material can be assumed as linear, isotropic, elastic and nearly incompressible. For this case, there are two main variables, the Young's Modulus E , and the Poisson's ratio ν .

From the parametric analysis, it is possible to see that the bulk modulus of this material does not possess a big impact in the FE simulation results. This conclusion combined with the results from the Poisson ratio in the first material model coincide with the statements from Bergström, where it is not vital to know these parameters to obtain accurate FE computational models, as these have limited influence on the mechanical response. [3]

6 Conclusion and Outlook

6.1 Summary and Contributions

6.2 Recommendations for Future Research

6.3 Conclusions and Final Remarks

A Frequently Asked Questions

A.1 How do I change the colors of links?

The color of links can be changed to your liking using:

```
\hypersetup{urlcolor=red}, or  
\hypersetup{citecolor=green}, or  
\hypersetup{allcolor=blue}.
```

If you want to completely hide the links, you can use:

```
\hypersetup{allcolors= .}, or even better:  
\hypersetup{hidelinks}.
```

If you want to have obvious links in the PDF but not the printed text, use:

```
\hypersetup{colorlinks=false}.
```


Bibliography

- [1] Nafiseh Ahanchian et al. "Estimating the material properties of heel pad sub-layers using inverse Finite Element Analysis". In: *Medical Engineering and Physics* 40 (2017), pp. 11–19. DOI: 10.1016/j.medengphy.2016.11.003.
- [2] "Ansys Mechanical APDL Element Reference". In: (Nov. 2010).
- [3] Jörgen Bergström. *Mechanics of Solid Polymers: Theory and Computational Modelling*. ISBN: 9780323311502.
- [4] FJ Carter et al. *Measurements and modelling of the compliance of human and porcine organs*. 2001, pp. 231–236. URL: www.elsevier.com/locate/media.
- [5] Chen Ket Chai et al. "Local axial compressive mechanical properties of human carotid atherosclerotic plaques-characterisation by indentation test and inverse finite element analysis". In: *Journal of Biomechanics* (2013). DOI: 10.1016/j.jbiomech.2013.03.017.
- [6] A. Chawla, S. Mukherjee, and B. Karthikeyan. "Characterization of human passive muscles for impact loads using genetic algorithm and inverse finite element methods". In: *Biomechanics and Modeling in Mechanobiology* (2009), pp. 67–76. DOI: 10.1007/s10237-008-0121-6.
- [7] Martijn A.J. Cox et al. "Mechanical characterization of anisotropic planar biological soft tissues using large indentation: A computational feasibility study". In: *Journal of Biomechanical Engineering* (3 June 2006), pp. 428–436. DOI: 10.1115/1.2187040.
- [8] Michael Drass et al. "Adhesive connections in glass structures—part I: experiments and analytics on thin structural silicone". In: *Glass Structures and Engineering* 3 (2018). DOI: 10.1007/s40940-017-0046-5.
- [9] Yuan Feng et al. "Characterizing white matter tissue in large strain via asymmetric indentation and inverse finite element modeling". In: *Journal of the Mechanical Behavior of Biomedical Materials* (2017), pp. 490–501. DOI: 10.1016/j.jmbbm.2016.09.020.
- [10] J. Sebastian Giudice et al. "Calibration of a Heterogeneous Brain Model Using a Subject-Specific Inverse Finite Element Approach". In: *Frontiers in Bioengineering and Biotechnology* (2021). DOI: 10.3389/fbioe.2021.664268.
- [11] Amirhossein Goharian, Seyed S.R. Koloor, and Mohamed R. Abdullah. *Biomechanical Evaluation Methods*. Elsevier Inc., 2017, pp. 65–87. DOI: 10.1016/B978-0-12-804634-0.00005-7.
- [12] Michelle Griffin et al. "Biomechanical characterization of human soft tissues using indentation and tensile testing". In: *Journal of Visualized Experiments* (Dec. 2016). DOI: 10.3791/54872.
- [13] Asif Husain, D. K. Sehgal, and R. K. Pandey. "An inverse finite element procedure for the determination of constitutive tensile behavior of materials using miniature specimen". In: *Computational Materials Science* (Sept. 2004), pp. 84–92. DOI: 10.1016/j.commatsci.2004.01.039.

- [14] Mikdam Jamal and Michael N. Morgan. "Characterization of material properties based on inverse finite element modelling". In: 4 (2019). ISSN: 24115134. DOI: 10.3390/inventions4030040.
- [15] J. Joseph et al. "Biomedical applications of polyurethane materials and coatings". In: *Transactions of the Institute of Metal Finishing* (May 2018), pp. 121–129. DOI: 10.1080/00202967.2018.1450209.
- [16] Valentine Kanyanta and Alojz Ivankovic. "Mechanical characterisation of polyurethane elastomer for biomedical applications". In: *Journal of the Mechanical Behavior of Biomedical Materials* 3 (Jan. 2010), pp. 51–62. DOI: 10.1016/j.jmbbm.2009.03.005.
- [17] M. Kauer et al. "Inverse finite element characterization of soft tissues". In: *Medical Image Analysis* 6 (2002), pp. 275–287.
- [18] David C. Lin et al. "Spherical indentation of soft matter beyond the Hertzian regime: Numerical and experimental validation of hyperelastic models". In: *Biomechanics and Modeling in Mechanobiology* (Oct. 2009), pp. 345–358. DOI: 10.1007/s10237-008-0139-9.
- [19] Kaifeng Liu, Mark R. VanLandingham, and Timothy C. Ovaert. "Mechanical characterization of soft viscoelastic gels via indentation and optimization-based inverse finite element analysis". In: *Journal of the Mechanical Behavior of Biomedical Materials* 2 (2009). DOI: 10.1016/j.jmbbm.2008.12.001.
- [20] Yuta Mori. "Development of a method for identifying the physical properties of post-extraction organs". In: (Feb. 2022).
- [21] R.W. Ogden. *Non-Linear Elastic Deformations*. Dover Civil and Mechanical Engineering. Dover Publications, 2013. ISBN: 9780486318714.
- [22] Thomas J. Pence and Kun Gou. "On compressible versions of the incompressible neo-Hookean material". In: *Mathematics and Mechanics of Solids* 20 (2 Feb. 2015), pp. 157–182. ISSN: 17413028. DOI: 10.1177/1081286514544258.
- [23] Padmanabhan Seshaiyer and Jay D. Humphrey. "A sub-domain inverse finite element characterization of hyperelastic membranes including soft tissues". In: *Journal of Biomechanical Engineering* (3 June 2003). ISSN: 01480731. DOI: 10.1115/1.1574333.
- [24] Lei Shi et al. "Anisotropic Material Characterization of Human Cervix Tissue Based on Indentation and Inverse Finite Element Analysis". In: *Journal of Biomechanical Engineering* (Sept. 2019). DOI: 10.1115/1.4043977.
- [25] Yue Sun et al. "Optimization method for the determination of Mooney-Rivlin material coefficients of the human breasts in-vivo using static and dynamic finite element models". In: *Journal of the Mechanical Behavior of Biomedical Materials* 90 (2019), pp. 615–625. DOI: 10.1016/j.jmbbm.2018.11.016.
- [26] Theodore Sussman and Klaus-Jürgen Bathe. "A finite element formulation for nonlinear incompressible elastic and inelastic analysis". In: *Computers and Structures* (1987), pp. 357–409. DOI: [https://doi.org/10.1016/0045-7949\(87\)90265-3](https://doi.org/10.1016/0045-7949(87)90265-3).
- [27] Wenshou Wang and Chun Wang. *Polyurethane for biomedical applications: A review of recent developments*. Elsevier, 2012, pp. 115–151. DOI: 10.1533/9781908818188.115.

- [28] Chen En Wu, Keng Hui Lin, and Jia Yang Juang. "Hertzian load-displacement relation holds for spherical indentation on soft elastic solids undergoing large deformations". In: *Tribology International* (May 2016), pp. 71–76. DOI: 10.1016/j.triboint.2015.12.034.
- [29] George Youssef. *Hyperelastic behavior of polymers*. 2022, pp. 117–144. DOI: 10.1016/b978-0-12-821078-9.00002-8.
- [30] Man Gong Zhang et al. "Spherical indentation method for determining the constitutive parameters of hyperelastic soft materials". In: *Biomechanics and Modeling in Mechanobiology* (1 2014), pp. 1–11. ISSN: 16177959. DOI: 10.1007/s10237-013-0481-4.
- [31] Sylwia D. Łagan and Aneta Liber-Kneć. "Experimental testing and constitutive modeling of the mechanical properties of the swine skin tissue". In: *Acta of Bioengineering and Biomechanics* 19 (2017). DOI: 10.5277/ABB-00755-2016-02.